Chemical Engineering Journal 462 (2023) 142202

Contents lists available at ScienceDirect

Chemical Engineering Journal

journal homepage: www.elsevier.com/locate/cej

Electrodeposited manganese oxides as efficient photocatalyst for the degradation of tetracycline antibiotics pollutant

Roberto Cestaro [a,b,*], Laetitia Philippe [a], Albert Serrà [a,c,d], Elvira Gómez [c,d], Patrik Schmutz [b,*]

[a] Empa Swiss Federal Laboratories for Materials Science and Technology, Laboratory for Mechanics of Materials and Nanostructures, CH-3602 Thun, Switzerland
[b] Empa Swiss Federal Laboratories for Materials Science and Technology, Laboratory for Joining Technologies and Corrosion, CH-8600 Dübendorf, Switzerland
[c] Grup d'Electrodeposició de Capes Primes i Nanoestructures (GE-CPN), Departament de Ciència de Materials i Química Física, Universitat de Barcelona, Barcelona, Catalonia, Spain
[d] Institute of Nanoscience and Nanotechnology (IN2UB), Universitat de Barcelona, Catalonia, Spain

ARTICLE INFO

Keywords:
Manganese oxides
Electrodeposition
Photocatalysis
Tetracycline antibiotics
Photocorrosion
Photomineralization mechanism

ABSTRACT

One of the important environmental challenges of the 21st century is the effective removal of pollutants from the aquatic environment. In this study, electrodeposited manganese oxides (Mn_yO_x) films were applied as visible-light-driven photocatalyst for the removal and mineralization of Tetracycline (TC) antibiotics. The photocatalytic activity of as-deposited and annealed Mn_yO_x was tested at different pH values using LED visible illumination, resulting in 92.4 % of TC mineralization efficiency after 180 min for the best performing manganese oxide. Quenching experiments showed that hydroxyl radicals ($^{\bullet}OH$) are the main active species responsible for the TC degradation. The photocorrosion of Mn_yO_x has been studied by quantifying the concentration of the dissolved manganese cations during the photocatalytic experiments. By comparing the catalyst mass loss with the % of TC mineralization, we revealed that the degradation of the oxide surface structure is the factor that, more than the photocorrosion, is limiting the photocatalytic activity of Mn_yO_x films. Finally, the photocatalytic mechanism of TC mineralization is proposed based on the detection of the intermediates species of the mineralization process by High-Performance Liquid Chromatography Mass-Spectroscopy. The facile synthesis process and the superior mineralization rate can open up a new approach for the possible large-scale utilization of electrodeposited Mn_yO_x films as an effective visible light photocatalyst.

1. Introduction

Nowadays antibiotics are widely used not only for human and animals medicine but also as additives in feedstuff industries. Tetracycline (TC) based antibiotics are the most common ones all over the world, accounting for about half of the global antibiotic production. However, TC is poorly adsorbed by animal metabolism and it is released into the environment in an active form. One of the serious problems related to its long-term presence in water and soil is the development of antimicrobial resistance in animals which potentially threatens ecosystem and human health [1–10]. The global antibiotic resistance problem has now reached an urgent point therefore research groups developed specific methods to efficiently remove TC from wastewater. These methods include: ultrasonic induced processes [11,12], electro-coagulation [13], advanced biological methods [14], adsorption [15–20] and photocatalytic degradation through advanced oxidation processes (AOP). Among them, photocatalytic AOP have attracted great interest thanks to their wide range of applications and high efficiency of pollutants mineralization. The generation of reactive oxygen species (ROS) such as hydroxyl radicals ($^{\bullet}OH$) or superoxide radicals ($^{\bullet}O_2^-$) during the AOP is mainly responsible for the degradation of refractive organic contaminants. Table S1 in the Supporting Information summarizes the principal studies dealing with the photocatalytic TC degradation, including key parameters such as photocatalyst type and dose, TC concentration, volume of reaction, pH, light source and intensity, and the results of the photocatalytic test in terms of percentage of TC mineralization in a determined amount of time. Most of the metal-based catalysts are unfortunately active only under ultra-violet irradiation, which represents only 5% of the sunlight radiation, and requires the use of high-energy consumption Xenon or UV lamps to be effective. To overcome

* Corresponding authors at: Empa Swiss Federal Laboratories for Materials Science and Technology, Laboratory for Joining Technologies and Corrosion, CH-8600 Dübendorf, Switzerland.
E-mail addresses: roberto.cestaro@empa.ch (R. Cestaro), patrik.schmutz@empa.ch (P. Schmutz).

https://doi.org/10.1016/j.cej.2023.142202
Received 2 December 2022; Received in revised form 14 February 2023; Accepted 26 February 2023
Available online 2 March 2023

these problems, manganese oxides (Mn_yO_x) have been considered as promising photocatalysts for the oxidative degradation of organic contaminants in wastewater due to the ease of synthesis, low-cost, non-toxic properties and strong adsorption and oxidation ability. Several investigations on the removal of aquatic pollutant by taking advantage of the high specific superficial area and the excellent adsorption properties of Mn_yO_x-based photocatalysts have been reported [21–27]. However, to the best of our knowledge, none of these studies deal with the mechanism of TC mineralization and the photocorrosion-related problematic of Mn_yO_x. In our previous study [28], we established a protocol for the reproducible preparation of Mn_yO_x with different stoichiometry and tailored semiconducting properties by combining electrodeposition and thermal annealing processes. Electrodeposition is one of the most suitable techniques for industrial preparation of Mn_yO_x since it requires low initial investments and provides high production rates offering control over the structure, composition and properties by simply adjusting parameters like applied potential, bath chemistry and temperature. The thermal annealing allowed the transformation in a specific crystal structure which significantly affected the light absorption. As example, an enhancement in the charge separation properties, reflected by nearly 40 % reduction in the photoluminescence peak intensity was evidenced for thermally treated Mn_yO_x in comparison with the as-electrodeposited samples. In addition, Tauc-plot analysis obtained from an UV–vis absorption spectra of Mn_yO_x revealed an energy gap (1.8 – 2.6 eV) suitable for visible light absorption. Based on these results, we report in this work the photocatalytic performances of as-deposited and annealed Mn_yO_x for the removal and degradation of TC antibiotic from water using LED visible light illumination. We monitored the mineralization of TC during 180 min by Total Organic Carbon (TOC) measurements in different pH conditions. Hydroxyl radicals ($^{\bullet}OH$) and superoxide radicals ($^{\bullet}O_2^-$) were determined as the reactive species affecting the TC photodegradation by quenching experiments and EPR measurements. The photocorrosion of the different manganese oxides is examined and future possible improvements of the photocatalysts durability are also discussed. Finally the TC degradation mechanism has been proposed based on the detection of intermediate products by HPLC-MS. These results provide a useful insight for the development of environmentally friendly manganese oxide-based photocatalytic systems.

2. Material and methods

2.1. Synthesis of Mn_yO_x films

The preparation of manganese oxide films with different stoichiometry was made according to our previous work [28]. Briefly, Mn_yO_x were synthetized by potentiostatic electrochemical deposition using a standard three-electrode electrochemical cell at room temperature. A deaerated electrolyte composed of 50 mM manganese acetate, $MnAc_2$ (Sigma Aldrich, > 98 %), and 100 mM sodium sulphate, Na_2SO_4 (Fluka, > 99.0 %) was used. A working electrode of Fluorine-doped Tin Oxide (FTO) covered glass (Sigma Aldrich, ~ 7 Ω/sq) was cleaned with soapy water and ultrasonicated for 10 min in deionized water, acetone and isopropanol prior the electrodeposition. A Pt wire and an Ag/AgCl 3 M KCl were used as counter and reference electrode, respectively. The electrodeposition was performed potentiostatically with an Autolab PGSTAT30 by applying a potential of 0.6 V or 1.0 V with a charge density of 2.0C/cm^2. After electrodeposition, the deposited layer was cleaned in 50 °C distilled water and dried in air flow at room temperature. Finally, a thermal treatment at 450 °C (5 °C/min) for 1 h in air atmosphere was performed using a rapid thermal annealing equipment (Advanced Riko Mila 5050).

2.2. Mn_yO_x photocatalysts characterization

Raman spectroscopy was used to investigate the chemical state of the as-deposited manganese oxides with a WITec Alpha 300 R confocal Raman microscope equipped with a 633 nm laser. The influence of the photocatalytic experiment on the morphology and the crystalline structure of Mn_yO_x was characterized by field-emission scanning electron microscopy (FE-SEM, Hitachi S-4800) and X-ray diffraction (XRD, Bruker D8 Discovery diffractometer) in the Bragg–Brentano configuration, Cu K_α radiation, respectively. The Brunauer–Emmett–Teller (BET) specific surface area was determined by the analysis of the nitrogen (77 K) adsorption–desorption isotherms measured using a Micrometrics Tristar-II system. For the determination of the BET specific surface area, the Mn_yO_x films were removed from the FTO-substrate and measured in form of powders.

2.3. Photocatalytic activity of Mn_yO_x films and TC degradation mechanism analysis

The photocatalytic activity of Mn_yO_x films was evaluated by degradation of a 50 ppm tetracycline, TC (Alfa Aesar, > 96 %) containing solution during 180 min of LED visible light irradiation (Power = 24.8 W, the wavelength domain is reported in Fig. S1 in the Supporting Information). Temperature, photocatalyst dosage, volume of polluted solutions, were fixed and maintained at 25 °C, 0.4 g/L, and 50 mL, respectively. The photocatalysts dose was determined by weighting the FTO-substrate before and after the electrodeposition of Mn_yO_x process and the eventual annealing treatment. The pH of the solution was adjusted to 4 or 6. Photolytic experiments were first performed in absence of photocatalyst for 180 min in the same irradiation conditions. The photolysis of TC was monitored by UV–vis spectroscopy (PerkinElmer Lambda 900 UV spectrophotometer). Before the photocatalytic experiments, polluted solutions were magnetically stirred in dark conditions for 1 h to reach the adsorption–desorption equilibrium. Additionally, 2.5 mL aliquots were collected for analysis at set time intervals during LED-light irradiation. Photocatalytic mineralization (i.e. degradation of TC into intermediate compounds and subsequently into CO_2 and H_2O) was also examined by comparing the total organic content prior to the start of irradiation and after stirring the pollutant solution for up to 180 min using a TOC analyzer (Shimadzu, model TOC-V_{CSH}). To investigate the role of the reactive species involved in the photocatalytic process (i.e., hydroxyl radicals, oxygen superoxide and photogenerated holes), the quenching of chemical selective radicals was performed. As an indicator, a pollutant solution of 50-ppm TC was used that contained (a) *tert*-Butanol (t-BuOH, Sigma-Aldrich, > 99.5 %), a quencher of hydroxyl radicals, (b) p-benzoquinone (PBQ, Sigma-Aldrich, > 98 %), a quencher of superoxide radicals, or (c) ammonium oxalate monohydrate (AO, Sigma-Aldrich, > 99 %), a quencher for photogenerated holes, which were independently added up to a concentration of 1 mM. The electronic spin resonance (ESR) spectra of DMPO (5,5-dimethyl-1-pyrroline N-oxide), a spin trapping reagent utilized to capture the superoxide ($^{\bullet}O_2^-$) and hydroxyl radicals ($^{\bullet}OH$), and TEMP (2,2,6,6-tetramethyl-4-piperidinol), utilized to trap singlet oxygen ($^1O_2$) were recorded using a Bruker 300E ESR spectrometer. High-Performance Liquid Chromatography Mass-Spectroscopy (HPLC-MS) was used to determine the photocatalytic degradation intermediates of TC (Waters Xevo G2-XS QToF system). The mobile phase was a 0.1% (v/v) formic acid aqueous solution. Elution was conducted at a flow rate of 0.2 mL min^{-1} and the injected volume was 2 μL. The linear gradient elution was changed from 90% formic acid aqueous solution and 10% of acetonitrile to a final 10% formic acid aqueous solution and 90% of acetonitrile within 4 min. An electrospray ionization source (capillary voltage, 4.0 kV; gas (N_2) flow rate; gas temperature, 300 °C) in a positive ion mode was used for MS. To investigate the Mn_yO_x photocorrosion, the total concentration of manganese ions in solution was determined using inductively coupled plasma-mass spectrometry (ICP-MS) measurements (PerkinElmer NexION 350D).

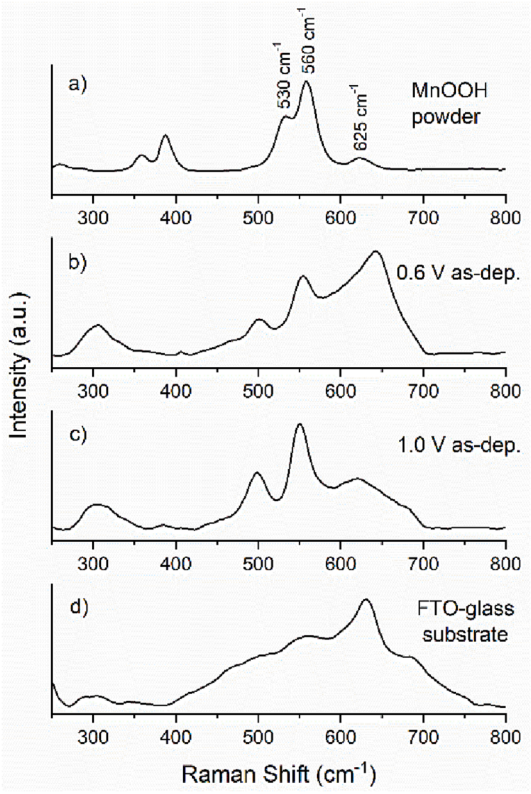

Fig. 1. Raman spectra of: a) MnOOH powder; b) 0.6 V as-deposited manganese oxide; c) 1.0 V as-deposited manganese oxide; d) FTO-glass substrate.

3. Results and discussion

3.1. Electrodeposited Mn_yO_x film characterization

Our previous study [28] established how to exert a precise control over the Mn_yO_x phase and morphology by adjusting the deposition parameters, especially by means of the applied potential. The as-electrodeposited manganese oxides were X-rays amorphous, while two different crystalline phases, Mn_3O_4 and Mn_2O_3, were obtained after the thermal treatment depending on the applied potential. In particular, the same heat treatment leads to the crystallization of a Mn_3O_4 phase when 0.6 V electrodeposition process was performed at 0.6 V or Mn_2O_3 when the applied potential was 1.0 V. This has been confirmed also by X-ray diffraction (XRD) and cross-sectional transmission electron microscopy (TEM) investigation through high-resolution TEM images, energy dispersive X-ray (EDX) color maps and selected-area electron diffraction (SAED) characterizations. However, given the initial amorphous nature and the high similarity between X-ray photoemission spectra (XPS) of Mn(II) and Mn(III) oxides, the determination of the stoichiometry of as-electrodeposited manganese oxides is still problematic. In this work, Raman spectroscopy was implemented to investigate the local chemical structure of the as-deposited amorphous manganese oxides. In Fig. 1, the Raman spectra of the 0.6 V and 1.0 V as-deposited manganese oxides together with the reference spectra of MnOOH powder and FTO-glass substrate are reported. The first-order vibrational energies of the reference MnOOH powder are labelled in the Raman spectrum a). Both the as-deposited manganese oxides show very similar Raman vibrational bands, with the only main difference being the band signal at ≈ 640 cm^{-1}, attributed to the presence of Mn_3O_4 phase. The shift in the wavenumber of the two main bands (500 – 560 cm^{-1}) with respect to the MnOOH powder is instead attributed to the effect of the Jan-Teller distortion, which is dominant in Mn(III) oxides [29,30].

To implement the Raman characterization with the previously reported XRD, XPS and cross-sectional TEM investigations [28], the chemical structures of the different manganese oxides are summarized as a function of the synthesis route in Table 1.

Table 1
Summary of the manganese oxides chemical structures depending on the synthesis conditions (applied potential and annealing treatment). The chemical structure of the annealed manganese oxides was determined by XRD, XPS and cross-sectional TEM investigation in ref. [28].

Applied potential	As-deposited	Annealed
0.6 V	MnOOH	Mn_3O_4
1.0 V	MnOOH	Mn_2O_3

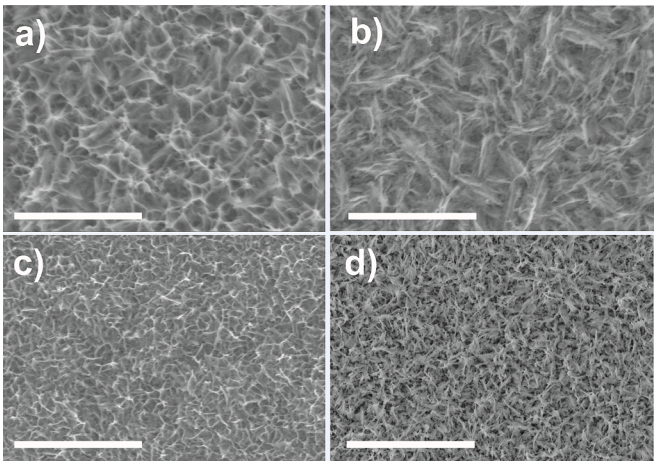

Fig. 2. SEM images of Mn_yO_x films: a) 0.6 V as-deposited; b) 0.6 V annealed; c) 1.0 V as-deposited; d) 1.0 V annealed. Scale bar: 1 μm.

Table 2
Morphological characteristics of annealed films.

Applied potential	Material	S_{BET} (m^2g^{-1})	V_{pore} (cm^3g^{-1})	D_{pore} (nm)
0.6 V	MnOOH (as deposited)	51	0.32	32
	Mn_3O_4 (annealed)	60	0.31	29
1.0 V	MnOOH (as deposited)	67	0.11	4
	Mn_2O_3 (annealed)	78	0.09	4

The surface morphology is one of the key factors affecting the catalytic performances. In Fig. 2, the SEM images of the different manganese oxides show the typical nanoflakes-like morphology in all the Mn_yO_x structures. At higher potential (Fig. 2 c) the nanoflakes are finer, according to the faster nucleation rate with respect to the nuclei growth, while at 0.6 V (Fig. 2 a) a coarser petal-shaped flakes morphology is developed. The effect of the annealing treatment on the surface morphology is almost negligible, although a subtle densification in the morphology is appreciated, as illustrated in Fig. 2 b) and d).

BET analysis was conducted to determine the morphological properties (effective surface area, porosity) of the different Mn_yO_x, N_2 adsorption–desorption isotherms. Table 2 shows the values of the BET specific surface area (S_{BET}), the pore volume (V_{pore}), and the average pore diameter (D_{pore}). The specific surface area of Mn_2O_3 films (78 m^2g^{-1}) is higher than that obtained for Mn_3O_4 (51 m^2g^{-1}). Note that larger specific surface areas are beneficial for providing abundant reaction sites and thus facilitating the adsorption of a higher amount of pollutant molecules on the catalyst surface. Without forgetting that many other factors could have a more pronounced influence on the photocatalytic degradation of TC, as mentioned later in this paper.

Table 3
Percentage of TC adsorption in dark conditions after 60 min of magnetic stirring.

Applied voltage (V)	Synthetic conditions	pH	TC adsorption (%)
0.6	As-dep.	4	3.4 ± 0.1
		6	1.2 ± 0.1
	Annealed	4	9.1 ± 0.2
		6	6.1 ± 0.2
1.0	As-dep.	4	1.7 ± 0.2
		6	1.8 ± 0.2
	Annealed	4	3.1 ± 0.2
		6	5.5 ± 0.2

3.2. Mn_yO_x photocatalytic activity and photocorrosion analysis

The UV–vis absorption peak of a TC solution (50 ppm) in absence of Mn_yO_x photocatalyst was monitored for 180 min during LED visible light irradiation, revealing a negligible photolysis of the refractive pollutant (Fig. S2, Supporting Information).

Prior starting the photocatalytic experiment, the pH 4 and pH 6 solutions with TC and Mn_yO_x photocatalyst films were magnetically stirred for 60 min in dark conditions to establish the adsorption–desorption equilibrium of TC on the surface of Mn_yO_x films. Table 3 summarizes the percentage values of TC adsorption at the adsorption–desorption equilibrium for the different samples and pH conditions.

Although deposited layers prepared at 1.0 V had larger specific surface areas than those prepared at 0.6 V, the surface with the highest adsorption capacity of TC was prepared at 0.6 V after annealing treatment. Heat treatment, and the consequent formation of crystalline Mn_3O_4 (0.6 V) and Mn_2O_3 (1.0 V) phases, leads to an increase of approximately 18% and 16% of the specific surface area, while the adsorption of TC is multiplied by approximately 2.7 times, at pH = 4.0, for deposits prepared at 0.6 V and approximately 3.1 times, at pH = 6.0, for films prepared at 1.0 V. Importantly, samples prepared at 0.6 V, both before and after annealing treatment, showed a higher capacity of adsorption at pH = 4, while in the case of deposits prepared at 1.0 V, the affinity between the surface of the photocatalyst and the TC is greater at pH = 6. It is known that the pH of the reacting media has a significant impact on the pollutants degradation mechanisms, as it affects the surface charge properties of both pollutant and photocatalyst [23,24,31]. In this work, the pHs of the reaction solution have been chosen based on the point of zero charge (*pzc*) of the Mn_yO_x photocatalyst and the pKa values of the TC pollutant. The protonation-deprotonation equilibrium of different Tetracycline functional groups depends on the pH: TC is fully protonated at pH ≈ 2, while it exists in a zwitterionic or anionic form in the pH range 3.3 – 7.0 or at pH > 7.7, respectively. Considering that manganese oxides have a *pzc* around pH 3.3, the choice of 4 and 6 pH media ensures an effective adsorption of the zwitterion pollutant on the negatively charged surface of the photocatalyst. On the other hand, the choice of a pH lower than 3.3 (where both Mn_yO_x and TC are positively charged on the surface) or a pH higher than 7.0 (where both Mn_yO_x and TC are negatively charged on the surface) would have prevented the adsorption of the pollutant on the photocatalyst. After reaching the adsorption–desorption equilibrium, the photocatalytic activities of Mn_yO_x oxides were evaluated by degrading a 50 ppm tetracycline solution with 0.4 g/L photocatalyst dose at room temperature and pH 4 or 6 under LED visible light irradiation. LED lights are up to 80% more efficient than traditional lighting such as Xenon and UV lamps and draw a much lower energy consumption [10]. 2.5 mL aliquots of polluted solutions were collected at set time intervals during the photocatalytic experiment for monitoring the TC mineralization by total organic carbon (TOC) measurements and the photocorrosion of the catalyst. In Fig. 3a)–b) is reported the variation with time of the TOC content normalized by the initial total organic carbon amount (TOC_0) for pH 4 and pH 6 solutions for the manganese oxides prepared at 0.6 V and 1.0 V, respectively. Additionally, the percentage of TC mineralization has been determined for each different experimental conditions, as shown in Fig. 3c)–d). It is important to note that some intermediate products of the pollutant degradation process might be equal or even more harmful than the initial organic pollutant. For this reason, the total percentage of pollutant mineralization is considered as the most relevant parameter describing the effective photocatalytic activity of a material. Both the TOC/TOC_0 and the TC mineralization analysis highlight the superior performances of the 1.0 V annealed Mn_2O_3 at pH 6. In detail, 92.4 % of TC mineralization was achieved after 180 min of LED visible light irradiation by Mn_2O_3, making it one of the best performing photocatalyst compared to other TC degradation studies (see Table S1 in the Supporting Information). The evaluation of TC mineralization percentages for the various Mn_yO_x photocatalysts operating in different pH conditions leads to the following considerations:

I. For both applied voltages (0.6 V or 1.0 V), the annealed Mn_yO_x exhibited the highest photocatalytic activity towards the mineralization of TC in a pH 6 TC solution.
II. Under the same experimental conditions, manganese oxides electrodeposited by applying 1.0 V have better photocatalytic performances than those electrodeposited at 0.6 V.

The photocorrosion of the different manganese oxides have been monitored during the photocatalytic mineralization of TC by ICP-MS determination of manganese concentration in solution at pH 4 and 6 and reported in Fig. 3e)–f). Values of low photocorrosion are obtained in the same conditions that yielded a high photocatalytic activity of the manganese oxides: 1.0 V deposition potential, implementation of annealing treatments and pH 6 solution. To further investigate the factors affecting the photocatalytic activity, the percentage of mass loss at the end of the photocatalytic experiment was determined for all the different Mn_yO_x photocatalysts and is reported in Fig. 4 together with the percentage of TC mineralization.

It is evident that the amount of dissolved photocatalysts is not the only responsible for the different photocatalytic performances of the Mn_yO_x films. Indeed, the same 2.1 % of mass loss was measured for the 0.6 V annealed manganese oxide (at pH 6) and the 1.0 V annealed manganese oxides (at pH 4), while the TC mineralization was 67.6 % and 37.2 %, respectively. This suggests that other factors, such as the oxide surface microstructure degradation, might play a major role towards the photocatalytic activity. To further corroborate this concept, the influence of the photocatalytic experiments on the surface morphology and the crystalline structures of Mn_yO_x has been investigated by FE-SEM and XRD. No relevant surface morphological changes were observed at the micrometer scale after the photocatalytic process by FE-SEM. To assess the structural modification induced by the photocatalytic process, X-ray diffractograms of the different manganese oxides before and after 180 min exposure to solution and LED-light irradiation are reported in Fig. 5. The following observation can be made: b) and f) diffractograms reveal the appearance of a broad peak at 31.6°, assigned to the MnOOH phase, after the photocatalytic experiment performed on the 0.6 V and 1.0 V as-deposited samples, respectively. The detection of MnOOH is consistent with the previous recorded Raman spectra of the amorphous manganese oxides (Fig. 1) suggesting a partial crystallization of the amorphous MnOOH matrix without a change in the oxide stoichiometry. This might be due to the dissolution of the amorphous MnOOH matrix and subsequent re-deposition of corrosion products of the same phase in a low crystalline state. A similar process has been already observed and reported a long time ago for other metal-oxide like Al_2O_3 [32]. Both d) and h) diffractograms denote a decrease in the peak intensity for the annealed crystalline structure samples deposited at 0.6 V Mn_3O_4 and 1.0 V Mn_2O_3, respectively. This manifests surface chemistry modifications with subsequent amorphization of the respective initially crystalline structure. Additionally, traces of MnOOH are detected in the X-ray diffraction patterns h) for the

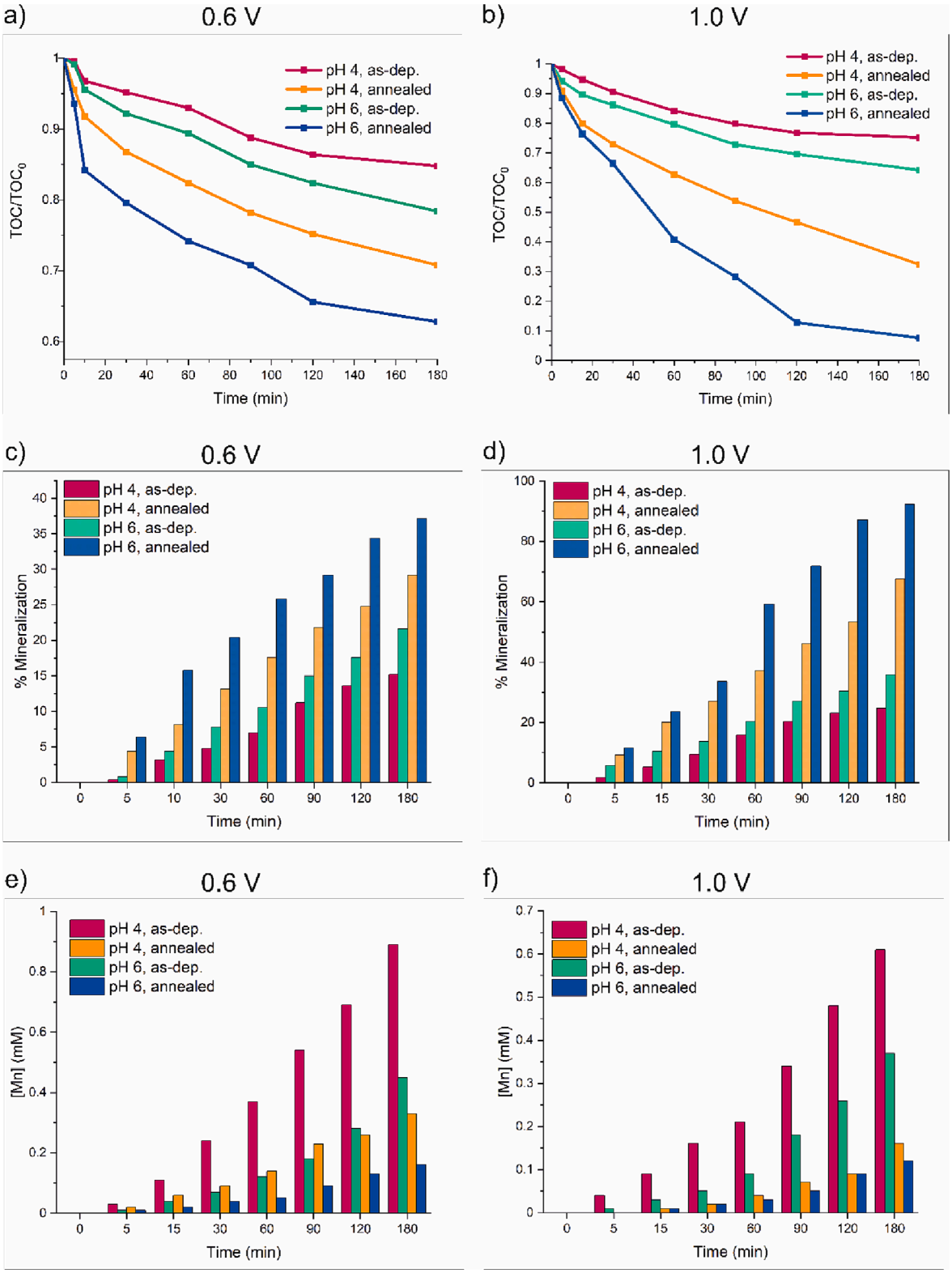

Fig. 3. Degradation of TC and Mn_yO_x photocatalysts' photocorrosion measured during the 180 min photocatalytic experiment (50 ppm TC solution with 0.4 g/L photocatalyst) under LED visible-light irradiation. All the measurements have been performed for the 0.6 V and 1.0 V as-deposited and annealed manganese oxides in condition of pH 4 and 6. a) - b) Total organic carbon content normalized by the initial total organic carbon amount. c) - d) Percentage of TC mineralization. e) - f) ICP-MS measurements of the total manganese cations concentration in solution.

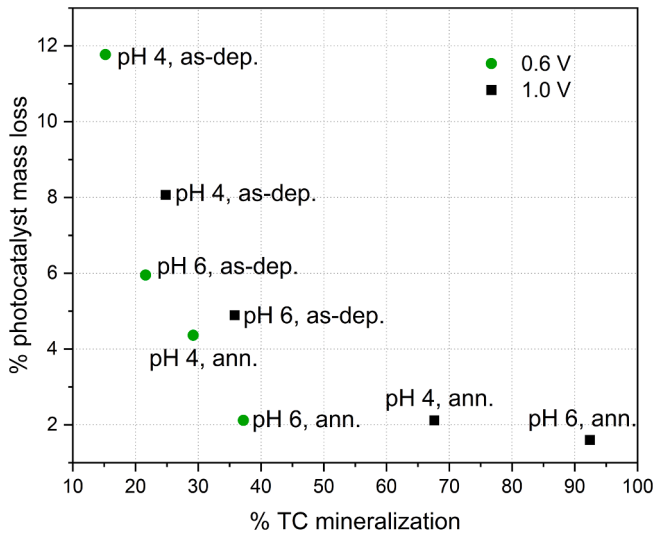

Fig. 4. Comparison of the photocatalytic performances of Mn_yO_x with respect to the percentage of photocatalyst mass loss after the 180 min photocatalytic experiment (50 ppm TC solution with 0.4 g/L photocatalyst) under LED visible-light irradiation.

deposited layer at 1.0 V subsequently annealed, revealing an oxide to hydroxide transformation of the compound by re-deposition of previously dissolved manganese species. Regarding the bump at 20–25° in the b), f) and h) diffractograms, we speculate its presence related to the presence of residuals organic compounds from the photocatalytic experiment. No structural modifications were observed in the FTO-glass substrate (diffractograms i-j).

The poor catalytic performances of amorphous as-deposited manganese oxides are therefore explained on the basis of a more critical microstructural degradation of the surface as well as a lower efficiency of light absorption. The same concepts also justify the superior performances of 1.0 V compared to 0.6 V Mn_yO_x, in accordance with our previous characterization of the oxide microstructural and semiconducting properties [28]. Our previous work [28] showed that the 1.0 V annealed Mn_2O_3 (the best performing sample in terms of photocatalytic activity and photocorrosion resistance) possesses the lowest band gap (1.8 eV) compared to the 1.0 V as-deposited (2.3 eV) and the 0.6 V as-deposited or annealed (2.5–2.6 eV) manganese oxides. Considering that the visible domain extends in the energy interval 1.8–3.2 eV (which corresponds to the wavelength range 700–380 nm), the red-shift in the band gap is extremely beneficial for the absorption of light in the whole visible range by the photocatalyst. Photoluminescence (PL) measurements provided useful additional information about the electron-hole recombination in the semiconducting Mn_yO_x photocatalyst. A low photoluminescence peak intensity indicates a low direct recombination in the semiconductor and thus better catalytic efficiency. Annealed Mn_yO_x revealed a reduction of up to 40% in the PL intensity with respect to the as-deposited Mn_yO_x counterpart. The 1.0 V annealed Mn_2O_3 showing the lowest PL intensity among all the other manganese oxides. Therefore, the highest photocatalytic activity of 1.0 V annealed Mn_2O_3 is explained on the basis of the synergy between: 1) larger visible light harvesting capability; 2) higher separation efficiency of photogenerated electron-hole pairs; 3) lower photocorrosion and degradation of the oxide surface microstructure (amorphization) during the photocatalytic process. Finally, the pH of the reaction media must also be

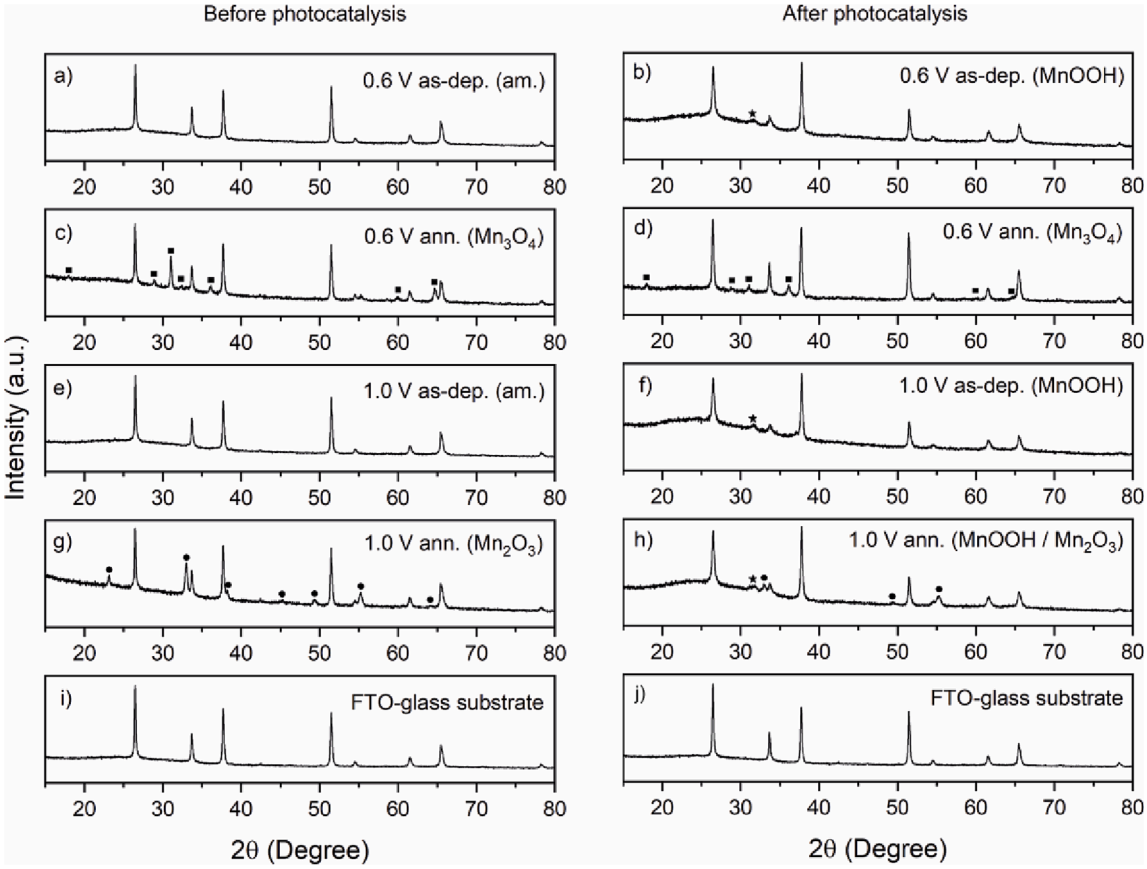

Fig. 5. X-ray diffractograms before and after 180 min of photocatalytic experiment (50 ppm TC solution with 0.4 g/L photocatalyst, pH 6 under LED visible light irradiation. a) - b) 0.6 V as-deposited, c) - d) 0.6 V annealed, e) - f) 1.0 V as-deposited and g) - h) 1.0 V annealed manganese oxides. i) FTO-glass substrate. Reference X-ray diffractograms are illustrated for MnOOH (star), Mn_3O_4 (square) and Mn_2O_3 (circle).

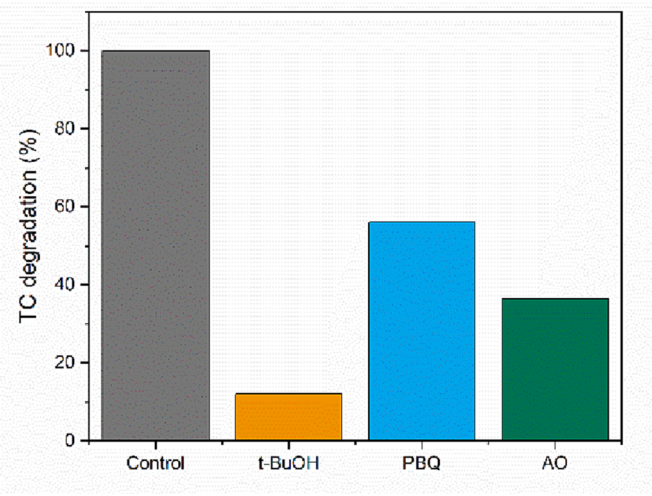

Fig. 6. Quenching of active species during the photocatalytic degradation of TC solutions (50 ppm, pH 6) by 1.0 V annealed Mn_2O_3 photocatalyst (0.4 g/L) after 180 min under LED visible light irradiation.

taken into consideration. Based on the Pourbaix diagram for the MnO_2-H_2O system [33], it is expected a greater stability of Mn_yO_x at pH 6 than at pH 4, thus also explaining the better photocatalytic performances (this being relevant as most of real waters show near neutral pH values). Similar pH-dependent results have been obtained in ref. [23]. The dissolution of solid manganese oxide into manganese cations (mostly Mn^{2+}, according to the Pourbaix diagram) happens also as a result of the interaction with the TC pollutant, emphasizing the role of Mn_yO_x as oxidizing agent [34]. Interestingly, the presence of Mn^{2+} in solution might even be beneficial: for example, Chen et al. demonstrated that dissolved Mn^{2+} cations promote TC degradation in presence of O_2 in alkaline conditions. Besides, using electrodeposited Mn_yO_x films, Mn^{2+} cations could be re-oxidized and deposited in form solid Mn_yO_x by repeating the electrodeposition process described in Section 2.1. These considerations reveal possible pathways for the further development of Mn_yO_x photocatalysts with extended durability achieved by reconditioning the electrode using the anodic electrodeposition process.

3.3. Determination of the reactive radical species

The identification of the most relevant active species involved during the TC mineralization was conducted by selective quenching of chemical radicals. In each of these experiments, a different quencher (either *tert*-Butanol - t-BuOH, p-benzoquinone - PBQ, or ammonium oxalate monohydrate - AO) was added to the polluted solution in presence of the 1.0 V annealed Mn_2O_3 photocatalyst. The percentage of TC mineralization obtained after 180 min under LED visible light irradiation in presence of each quencher is reported in Fig. 6.

The addition of t-BuOH (scavenger of hydroxyl radicals, $^{\bullet}OH$) in the reaction system significantly inhibited the TC degradation, while PBQ and AO (scavengers of superoxide radicals, $^{\bullet}O_2$, and holes, h^+, respectively) had less influence on the photocatalytic performances of the 1.0 V annealed Mn_2O_3 photocatalyst.

These results suggest that under these photocatalytic conditions, the hydroxyl radicals are the dominant active species responsible for the TC degradation. However, from Fig. 6, it can also be recognized that the presence/absence of superoxide radicals and holes has a non-negligible

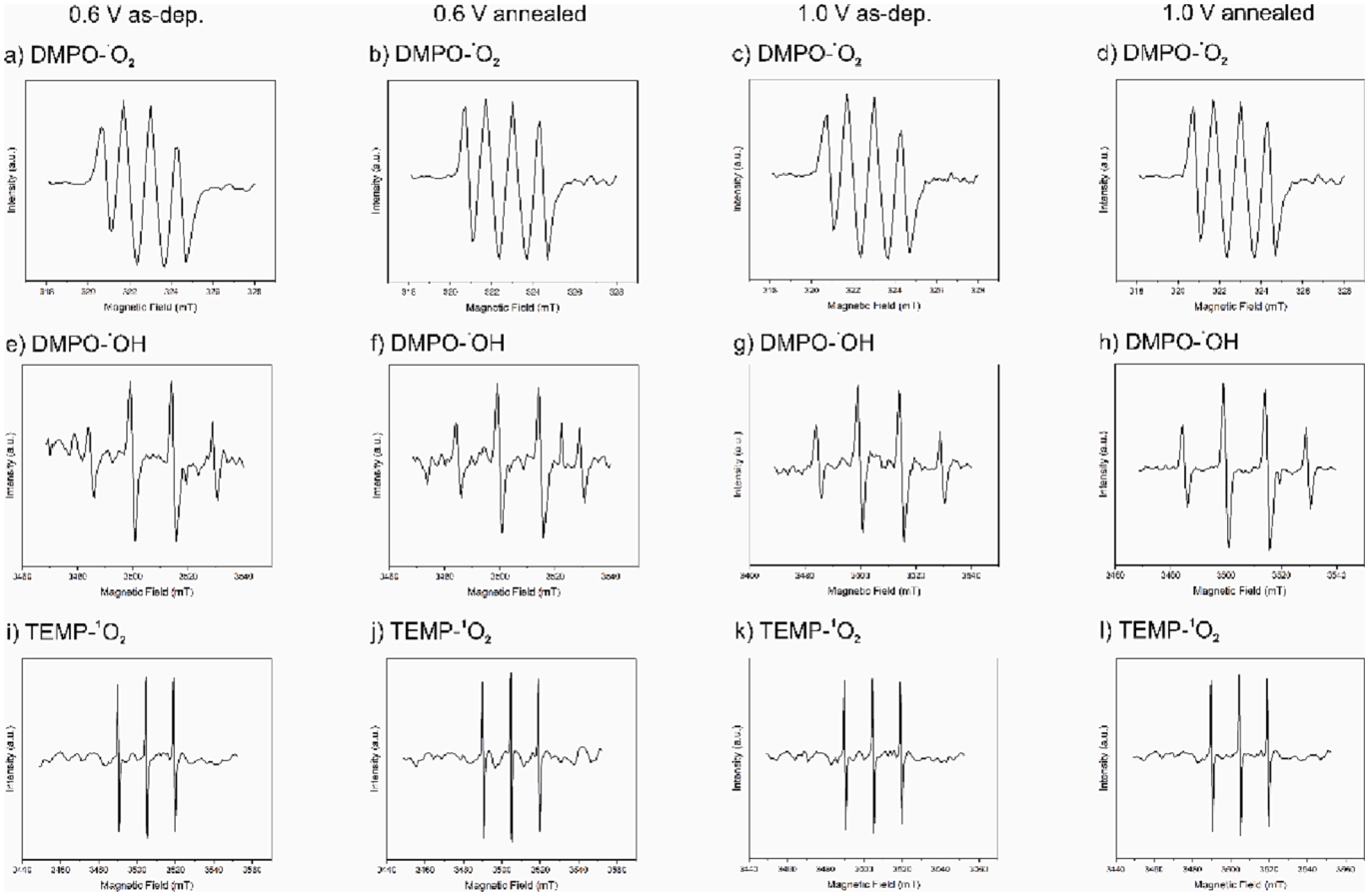

Fig. 7. ESR spectra of a-d) DMPO-$^{\bullet}O_2$; e-h) DMPO-$^{\bullet}OH$; i-l) TEMP-$^1O_2$ with 0.6 V and 1.0 V as-deposited and annealed photocatalysts during LED visible light irradiation.

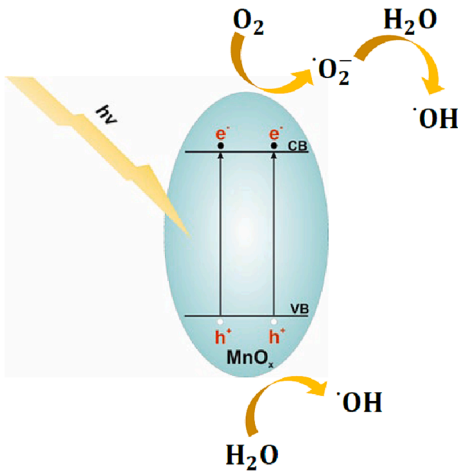

Fig. 8. Proposed mechanism for the generation of hydroxyl radicals by visible light irradiation of Mn_yO_x.

effect on the photolysis process. ESR spin-trap experiments were carried out in DMPO and TEMP to further investigate the role of $^{\cdot}O_2$, $^{\cdot}OH$ and singlet oxygen ($^1O_2$), respectively. The ESR spectra for as-deposited at 0.6 V or 1.0 V and annealed manganese oxides are reported in Fig. 7. The following characteristic signals have been identified: a) and d) $^{\cdot}O_2$, 4 peaks with 1:1:1:1 intensity ratio; e) and h) $^{\cdot}OH$, 4 peaks with 1:2:2:1 intensity ratio; i) and n) $^1O_2$, 3 peaks with 1:1:1 intensity ratio. Therefore, all of these species were produced during the photocatalytic experiment and played a major role in the photodegradation process. The presence of singlet oxygen supports evidence of a non-radical pathway for the TC degradation.

Based on the quenching experiments and ESR results, a possible mechanism for the generation of the reactive radical species under visible light irradiation of Mn_yO_x is proposed (Fig. 8). The band gap of Mn_yO_x (1.8–2.5 eV [28]) allows the absorption of visible light, which lead to the promotion of electrons in the conduction band (CB) and the simultaneous formation of holes in the valence band (VB). Photogenerated electrons might react with dissolved/adsorbed O_2 to form $^{\cdot}O_2$. The main role of superoxide radicals is expected to be the formation of $^{\cdot}OH$ upon reaction with water protons due to the low oxidation power of $^{\cdot}O_2$ compared with $^{\cdot}OH$. On the other hand, $^{\cdot}OH$ are also generated via water hydrolysis by photogenerated h^+. As a consequence, the

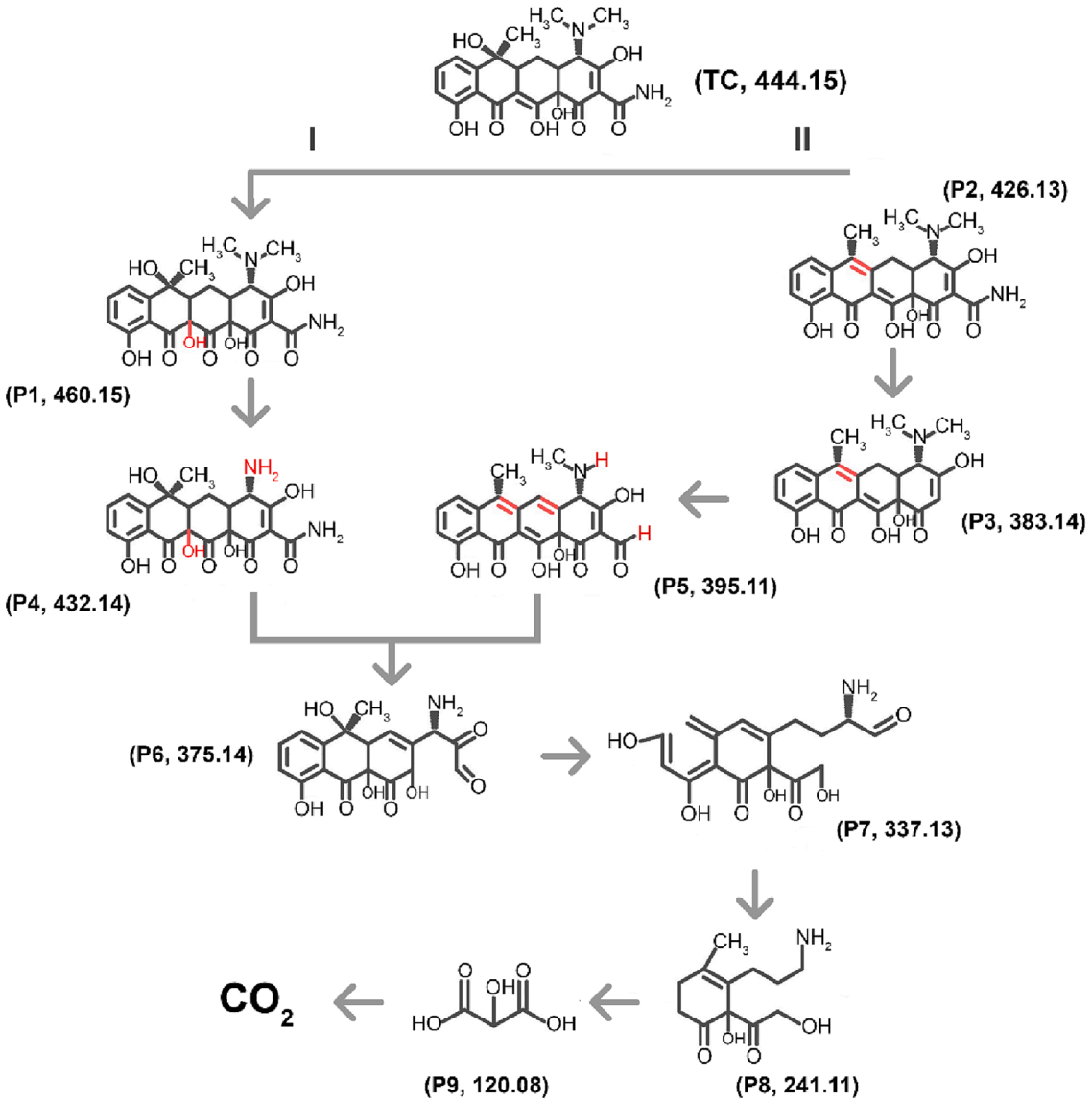

Fig. 9. Proposed photocatalytic degradation pathway of TC.

photocatalytic activity of the different Mn_yO_x is directly dependent on the ability of $^{\bullet}OH$ generation, which is then reflected in the light absorption and the electron-holes pairs recombination processes. Based on photoluminescence measurements [28] and the above mentioned results, the superior photocatalytic performance of annealed Mn_yO_x is also attributed to the formation of crystalline structures that ensure better light harvesting properties (band gap reduction) and a prolonged lifetime of photogenerated e^-- h^+ pairs.

3.4. TC degradation mechanism

To gain a deeper understanding of the photomineralization process of TC on Mn_yO_x photocatalyst surfaces using visible LED light, the presence of intermediate products during degradation of TC was detected and identified by HPLC–MS analysis. The initial strong signal of mass/charge (m/z) at $m/z = 444$ corresponds to TC. The detected intermediates are generated mainly through demethylation, dehydroxylation, deamidation, and ring-opening reactions. Based on the identified degradation molecules, two justifiable TC degradation pathways were proposed and depicted in Fig. 9. For pathway I, hydroxylated product P1 ($m/z = 460$) is formed via an electrophilic addition of –OH; this is followed by the successive demethylation of the amine group, resulting in product P4 ($m/z = 432$), which is subsequently decomposed into product P6 ($m/z = 375$) by breaking the cyclic hydrocarbon structure. This is in agreement with previously reported studies [23,35,36]. In pathway 2, the intermediate P2 ($m/z = 426$) is formed by TC dehydration, which is further oxidized via deamidation, demethylation, and dehydroxylation, resulting in the formation of the intermediates P3 ($m/z = 383$), P5 ($m/z = 395$), and P6 ($m/z = 375$). Further oxidation reactions by hydroxyl radicals, including C-C bond breakage, lead to the mineralization of these TC intermediates to shorter carboxylic acids chains and finally to complete mineralization.

4. Conclusion

In this work, we applied electrodeposited Mn_yO_x films as visible-light-driven photocatalyst for the removal and mineralization of TC antibiotics. The morphological properties were characterized by SEM denoting a nanoflake-like surface morphology and BET analysis evidenced a large specific surface area (51–78 m^2g^{-1}), both beneficial for catalytic applications. The highest percentage of TC degradation (92.4 %) was obtained with the 1.0 V annealed Mn_2O_3 at pH 6 after 180 min of LED visible light irradiation. We determined multiple factors affecting the photocatalytic activities of Mn_yO_x films, here summarized as follows:

1) Microstructural stability. XRD analysis revealed that during the photocatalytic process the Mn_yO_x surface suffered from amorphization of the crystalline structure as well as dissolution / re-deposition of MnOOH phase. In this context, the development of a crystalline structure after the annealing and the near neutral pH conditions (pH 6) are beneficial to reduce the surface degradation and the photocorrosion of Mn_yO_x films.
2) Ability of $^{\bullet}OH$ radicals generation. Quenching experiments demonstrated that $^{\bullet}OH$ radicals are the main active species responsible for the degradation of TC. The mechanism for the generation of the reactive radicals has been proposed based on the EPR analysis and our previous investigation on the semiconducting properties of electrodeposited Mn_yO_x films [28]. The generation of $^{\bullet}OH$ radicals is dependent on the visible light harvesting ability and the separation efficiency of photogenerated electron-hole pairs, both enhanced by the crystalline structure of 1.0 V annealed Mn_2O_3.

Finally, we proposed a TC degradation pathway based on the detection of the intermediates products during the mineralization process of TC by HPLC–MS analysis, proving at the same time the absence of stable harmful side-products. The presented findings shed a light on the correlation between the corrosion mechanism and the surface oxide reactivity of different Mn_yO_x films, which serves as a basis to develop new strategies to improve the photocatalytic performances and the photocorrosion resistance of manganese oxides-based catalysts.

Declaration of Competing Interest

The authors declare that they have no known competing financial interests or personal relationships that could have appeared to influence the work reported in this paper.

Data availability

Data will be made available on request.

Acknowledgments

The work has been performed within the frame of the following Grant PID2020-115663GB-C32 funded by MCIN/AEI/10.13039/501100011033. Authors thank the CCiT-UB for the use of their equipment and Metrohm foundation for the financial support of this research

Appendix A. Supplementary data

Supplementary data to this article can be found online at https://doi.org/10.1016/j.cej.2023.142202.

References

[1] T.P. Van Boeckel, J. Pires, R. Silvester, C. Zhao, J. Song, N.G. Criscuolo, M. Gilbert, S. Bonhoeffer, R. Laxminarayan, Global trends in antimicrobial resistance in animals in low- And middle-income countries, Science 80- (2019) 365, https://doi.org/10.1126/science.aaw1944.
[2] M.B. Ahmed, J.L. Zhou, H.H. Ngo, W. Guo, Adsorptive removal of antibiotics from water and wastewater: Progress and challenges, Sci. Total Environ. 532 (2015) 112–126, https://doi.org/10.1016/j.scitotenv.2015.05.130.
[3] Y. Dai, M. Liu, J. Li, S. Yang, Y. Sun, Q. Sun, W. Wang, L. Lu, K. Zhang, J. Xu, W. Zheng, Z. Hu, Y. Yang, Y. Gao, Z. Liu, A review on pollution situation and treatment methods of tetracycline in groundwater, Sep. Sci. Technol. 55 (2020) 1005–1021, https://doi.org/10.1080/01496395.2019.1577445.
[4] T. Deblonde, C. Cossu-Leguille, P. Hartemann, Emerging pollutants in wastewater: A review of the literature, Int. J. Hyg. Environ. Health. 214 (2011) 442–448, https://doi.org/10.1016/j.ijheh.2011.08.002.
[5] V. Homem, L. Santos, Degradation and removal methods of antibiotics from aqueous matrices - A review, J. Environ. Manage. 92 (2011) 2304–2347, https://doi.org/10.1016/j.jenvman.2011.05.023.
[6] S. Rodriguez-Mozaz, S. Chamorro, E. Marti, B. Huerta, M. Gros, A. Sànchez-Melsió, C.M. Borrego, D. Barceló, J.L. Balcázar, Occurrence of antibiotics and antibiotic resistance genes in hospital and urban wastewaters and their impact on the receiving river, Water Res. 69 (2015) 234–242, https://doi.org/10.1016/j.watres.2014.11.021.
[7] B.W. Schwab, E.P. Hayes, J.M. Fiori, F.J. Mastrocco, N.M. Roden, D. Cragin, R. D. Meyerhoff, V.J. D'Aco, P.D. Anderson, Human pharmaceuticals in US surface waters: A human health risk assessment, Regul. Toxicol. Pharmacol. 42 (2005) 296–312, https://doi.org/10.1016/j.yrtph.2005.05.005.
[8] J. Rivera-Utrilla, M. Sánchez-Polo, M.Á. Ferro-García, G. Prados-Joya, R. Ocampo-Pérez, Pharmaceuticals as emerging contaminants and their removal from water. A review, Chemosphere 93 (2013) 1268–1287, https://doi.org/10.1016/j.chemosphere.2013.07.059.
[9] A.J. Watkinson, E.J. Murby, S.D. Costanzo, Removal of antibiotics in conventional and advanced wastewater treatment: Implications for environmental discharge and wastewater recycling, Water Res. 41 (2007) 4164–4176, https://doi.org/10.1016/j.watres.2007.04.005.
[10] A. Serrà, L. Philippe, F. Perreault, S. Garcia-Segura, Photocatalytic treatment of natural waters. Reality or hype? The case of cyanotoxins remediation, Water Res. 188 (2021) 116543.
[11] Y. Wang, H. Zhang, L. Chen, Ultrasound enhanced catalytic ozonation of tetracycline in a rectangular air-lift reactor, Catal. Today. 175 (2011) 283–292, https://doi.org/10.1016/j.cattod.2011.06.001.
[12] L. Hou, H. Zhang, L. Wang, L. Chen, Ultrasound-enhanced magnetite catalytic ozonation of tetracycline in water, Chem. Eng. J. 229 (2013) 577–584, https://doi.org/10.1016/j.cej.2013.06.013.
[13] C. Dai, S. Shi, D. Chen, J. Liu, L. Huang, J. Zhang, Y. Feng, Study on the mechanism of tetracycline removal in electrocoagulation coupled with electro-fenton reaction system with Fe anode and carbon nanotube cathode, Chem. Eng. J. 428 (2022), 131045, https://doi.org/10.1016/j.cej.2021.131045.

[14] S. Aydin, B. Ince, O. Ince, Development of antibiotic resistance genes in microbial communities during long-term operation of anaerobic reactors in the treatment of pharmaceutical wastewater, Water Res. 83 (2015) 337–344, https://doi.org/10.1016/j.watres.2015.07.007.
[15] A.C. Martins, O. Pezoti, A.L. Cazetta, K.C. Bedin, D.A.S. Yamazaki, G.F.G. Bandoch, T. Asefa, J.V. Visentainer, V.C. Almeida, Removal of tetracycline by NaOH-activated carbon produced from macadamia nut shells: Kinetic and equilibrium studies, Chem. Eng. J. 260 (2015) 291–299, https://doi.org/10.1016/j.cej.2014.09.017.
[16] T. Wang, L. Xue, Y. Liu, T. Fang, L. Zhang, B. Xing, Insight into the significant contribution of intrinsic defects of carbon-based materials for the efficient removal of tetracycline antibiotics, Chem. Eng. J. 435 (2022), 134822, https://doi.org/10.1016/j.cej.2022.134822.
[17] L. Zhang, X. Song, X. Liu, L. Yang, F. Pan, J. Lv, Studies on the removal of tetracycline by multi-walled carbon nanotubes, Chem. Eng. J. 178 (2011) 26–33, https://doi.org/10.1016/j.cej.2011.09.127.
[18] Y. Gao, Y. Li, L. Zhang, H. Huang, J. Hu, S.M. Shah, X. Su, Adsorption and removal of tetracycline antibiotics from aqueous solution by graphene oxide, J. Colloid Interface Sci. 368 (2012) 540–546, https://doi.org/10.1016/j.jcis.2011.11.015.
[19] P. Arabkhani, A. Asfaram, The potential application of bio-based ceramic/organic xerogel derived from the plant sources: A new green adsorbent for removal of antibiotics from pharmaceutical wastewater, J. Hazard. Mater. 429 (2022), 128289, https://doi.org/10.1016/j.jhazmat.2022.128289.
[20] Z. Salmanzadeh-Jamadi, A. Habibi-Yangjeh, S.R. Pouran, X. Xu, C. Wang, Facile fabrication of TiO2/Bi5O7Br photocatalysts for visible-light-assisted removal of tetracycline and dye wastewaters, J. Phys. D. Appl. Phys. 55 (16) (2022) 165105.
[21] Y.a. Cheng, Y. Zhang, W. Xiong, T. Huang, Simultaneous removal of tetracycline and manganese (II) ions from groundwater using manganese oxide filters: Efficiency and mechanisms, J. Water Process Eng. 42 (2021) 102158.
[22] W.T. Jiang, P.H. Chang, Y.S. Wang, Y. Tsai, J.S. Jean, Z. Li, Sorption and desorption of tetracycline on layered manganese dioxide birnessite, Int. J. Environ. Sci. Technol. 12 (2015) 1695–1704, https://doi.org/10.1007/s13762-014-0547-6.
[23] P. Mahamallik, S. Saha, A. Pal, Tetracycline degradation in aquatic environment by highly porous MnO2 nanosheet assembly, Chem. Eng. J. 276 (2015) 155–165, https://doi.org/10.1016/j.cej.2015.04.064.
[24] Z. Song, Y.L. Ma, C.E. Li, The residual tetracycline in pharmaceutical wastewater was effectively removed by using MnO2/graphene nanocomposite, Sci. Total Environ. 651 (2019) 580–590, https://doi.org/10.1016/j.scitotenv.2018.09.240.
[25] H. Wang, D. Zhang, S. Mou, W. Song, F.A. Al-Misned, M.G. Mortuza, X. Pan, Simultaneous removal of tetracycline hydrochloride and As(III) using poorly-crystalline manganese dioxide, Chemosphere 136 (2015) 102–110, https://doi.org/10.1016/j.chemosphere.2015.04.070.
[26] D. Wang, F. Jia, H. Wang, F. Chen, Y. Fang, W. Dong, G. Zeng, X. Li, Q. Yang, X. Yuan, Simultaneously efficient adsorption and photocatalytic degradation of tetracycline by Fe-based MOFs, J. Colloid Interface Sci. 519 (2018) 273–284, https://doi.org/10.1016/j.jcis.2018.02.067.
[27] G. Lv, X. Xing, L. Liao, P. An, H. Yin, L. Mei, Z. Li, Synthesis of birnessite with adjustable electron spin magnetic moments for the degradation of tetracycline under microwave induction, Chem. Eng. J. 326 (2017) 329–338, https://doi.org/10.1016/j.cej.2017.05.123.
[28] R. Cestaro, P. Schweizer, L. Philippe, X. Maeder, A. Serrà, Phase and microstructure control of electrodeposited Manganese Oxide with enhanced optical properties, Appl. Surf. Sci. 580 (2022) 152289.
[29] C.M. Julien, M. Massot, C. Poinsignon, Lattice vibrations of manganese oxides: Part I. Periodic structures, Spectrochim. Acta - Part A Mol. Biomol. Spectrosc. 60 (2004) 689–700, https://doi.org/10.1016/S1386-1425(03)00279-8.
[30] S. Bernardini, F. Bellatreccia, G. Della Ventura, A. Sodo, A reliable method for determining the oxidation state of manganese at the microscale in Mn oxides via Raman spectroscopy, Geostand. Geoanal. Res. 45 (1) (2021) 223–244.
[31] J. Wu, H. Zhang, N. Oturan, Y. Wang, L. Chen, M.A. Oturan, Application of response surface methodology to the removal of the antibiotic tetracycline by electrochemical process using carbon-felt cathode and DSA (Ti/RuO2-IrO2) anode, Chemosphere 87 (2012) 614–620, https://doi.org/10.1016/j.chemosphere.2012.01.036.
[32] R.S. Alwitt, The Growth of Hydrous Oxide Films on Aluminum, J. Electrochem. Soc. 121 (1974) 1322, https://doi.org/10.1149/1.2401679.
[33] M. Pourbaix, Atlas of Electrochemical Equilibria in-Aqueous Solutions, Pergamon Press, Oxford, 1966.
[34] G. Chen, L. Zhao, Y., hua, Dong,, Oxidative degradation kinetics and products of chlortetracycline by manganese dioxide, J. Hazard. Mater. 193 (2011) 128–138, https://doi.org/10.1016/j.jhazmat.2011.07.039.
[35] M. Arif, T. Muhmood, M. Zhang, M. Amjad Majeed, Y. Honglin, X. Liu, X. Wang, Highly visible-light active, eco-friendly artificial enzyme and 3D Bi4Ti3O12 biomimetic nanocomposite for efficient photocatalytic tetracycline hydrochloride degradation and Cr(VI) reduction, Chem. Eng. J. 434 (2022) 1–16, https://doi.org/10.1016/j.cej.2021.134491.
[36] J. Liu, H.e. He, Z. Shen, H.H. Wang, W. Li, Photoassisted highly efficient activation of persulfate over a single-atom Cu catalyst for tetracycline degradation: Process and mechanism, J. Hazard. Mater. 429 (2022) 128398.